

Unsteady Thermodynamic CFD Simulations of Aircraft Wing Anti-Icing Operation

Jun Hua*, Fanmei Kong⁺, Hugh H.T. Liu[†]
Institute for Aerospace Studies, University of Toronto
4925 Dufferin Street, Toronto, Ontario, M3H 5T6, Canada

ABSTRACT

A three-dimensional unsteady thermodynamic simulation model is developed to describe the dynamic response of an aircraft wing anti-icing system. This computational fluid dynamics based model involves a complete wing segment including thermal anti-icing bay inside the leading edge. The unsteady, integrated internal/external thermal flow simulation is presented with heat conductivity through the solid skin in a structured mesh. The calculated skin temperature results are satisfactory in their good match with flight test data. The presented research work indicates a strong potential of using computational fluid dynamics in dynamic wing anti-icing system model development and validation.

*Research Associate

⁺Visiting Scientist, Beijing University of Aeronautics and Astronautics

[†] Associate Professor and corresponding author, liu@utias.utoronto.ca

Nomenclature

| | | |
|----------------|---|--------------------------|
| M | = | Mach number |
| P, p | = | static pressure (Pa) |
| P _o | = | total pressure (Pa) |
| t | = | time (sec) |
| T | = | static temperature (K) |
| T _o | = | total temperature (K) |
| U | = | velocity (m/sec) |
| α | = | angle of attack (degree) |

1. Introduction

The research background comes from the necessity of developing a dynamic control technique for aircraft wing anti-icing system (WAIS). Fig. 1 shows a typical flowchart of such a system. The hot air from the turbo engine is introduced to the leading edge through pipes and valves. The control module regulates the wing anti-icing valve (WAIV) to control the heat flux into the Piccolo tubes in the leading edge anti-icing bays. It in turn adjusts the skin temperature of the wing leading edge. The control system works in a closed loop with the temperature sensors located at several points of the wing leading edge surface.

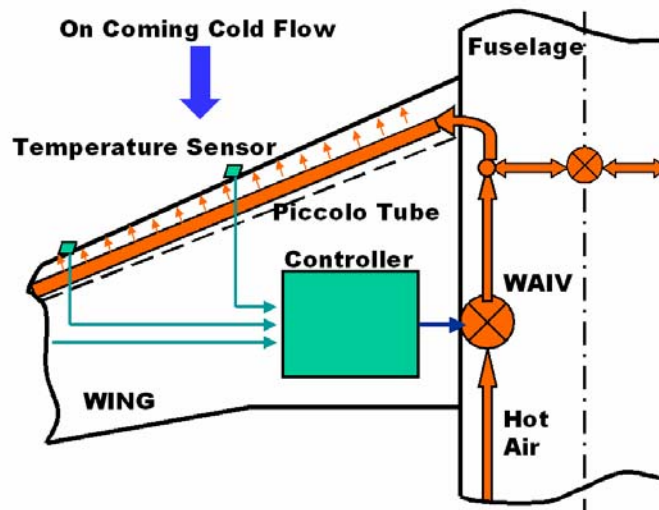


Fig. 1 Flowchart of a WAIS (left hand side only)

An efficient wing anti-icing control system development requires a dynamic thermal fluid model. It is a challenging task due to its complicated physics behavior in both anti- and de-icing flight operations. One well-received approach is to develop an empirical dynamic model of parameters that are tuned by flight test data, which are expensive and difficult to obtain, and even impossible in the early design phase. Instead, our research explores using

the computational fluid dynamics (CFD) simulation data to assist in dynamic model development. Obviously unsteady simulations are required to serve this purpose.

CFD has been used in anti-icing research for years. Topics of recent work are mainly covered in the following two categories: 1) the CFD methods and software development to simulate the ice accretion process in external airflows with cold droplets. Research work includes FENSAP-ICE (Habashi et al 2000¹, 2003²), LEWICE3D, ICEGRID3D, and CMARC (Bidwell et al 1999³); 2) application of available CFD tools for aircraft anti-icing device design. Typical work includes Morency et al (2000)⁴, and de Mattos and Oliveira (2000)⁵. The authors of this paper also presented their earlier work in steady Navier-Stokes simulations of the integrated internal/external thermodynamic simulations of two dimensional (2D) wing sections and three dimensional (3D) wing segment with WAIS (Liu and Hua 2004⁶ and 2005⁷). Structured meshes were generated for both hot internal bleeding air and cold external fields with heat conductivity through the wing skin. Simulation results visually revealed the hot/cold flow interactions and heat conductivity through the fluid and solid zones. Such steady CFD simulations provided useful observations for WAIS research and development.

In this paper, the 2D unsteady CFD simulations are first studied for time-dependent computations of WAIS under different hot air inlet conditions. They simulate the thermal flow under the adjustment of the control valves, and calculate the corresponding skin temperature. Then the 3D unsteady CFD model of WAIS is analysed to simulate a complete anti-icing flight test loop. The calculated skin temperature results are found to coincide with the flight measurement very well. Therefore, the unsteady simulation results may be used in dynamic model tuning to complement or even re-create a flight test process.

2. Model Description

The 3D wing span segment (Fig. 2 & 3) consists of the following components. 1) A Piccolo tube introduces the hot air into the leading edge anti-icing bay. There are a number of small hoses on the front side of the Piccolo tube from where the hot jets impinge the inner surface of the leading edge. The small holes are located staggered in two rows of angles 15° upper and lower from the wing chord plane. 2) The aluminium skin is heated by the hot air in the anti-icing operation. 3) Two exhaust holes on the lower side of the bay allow the hot air to exit to the external flow. 4) Two ribs separate the bays in the span direction with the hoses on the ribs neglected. 5) The heat shield serves as the back wall of the bay.

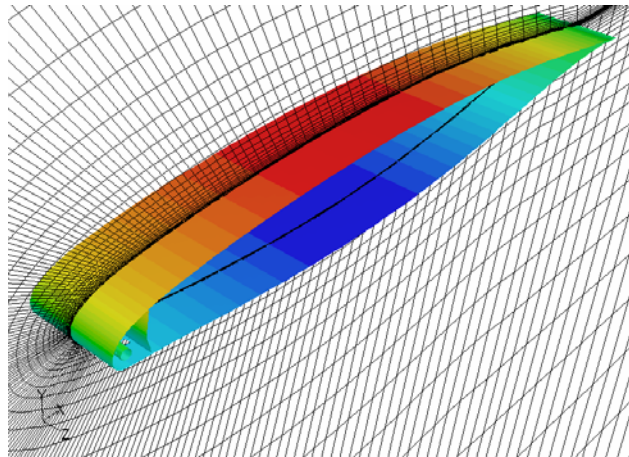


**Fig. 2 Wing segment with the thermal anti-icing bay
(Shown with the mesh of a mid-span plane)**

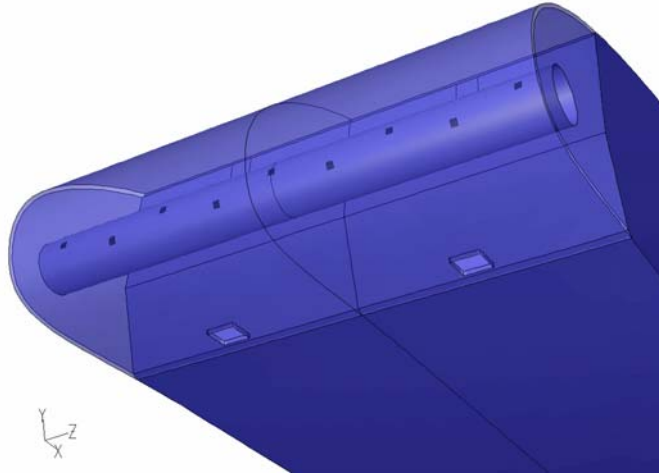


Fig. 3 Leading edge anti-icing bay details

Structured meshes are generated for both internal and external flow fields. The interior and exterior meshes are connected through the mesh in the exhaust holes. A structured mesh is also used inside the aluminium skin for the heat conductivity calculation. The higher computational efficiency of the structured mesh made it possible to conduct the 3D unsteady simulation on a common PC, which has a single Intel Pentium processor, 1G memory and 80G hard disk.

For the initial steps of this investigation, a 2D model representing a span section of this wing segment is also generated.

3. Unsteady Thermodynamic Simulations

3.1. The Navier-Stokes Solver

The CFD method used in this research is a well-known Navier-Stokes solver FLUENT V6.1/6.2⁸. Its reliability has been demonstrated by a great number of aerospace and industrial applications.

3.2. The Boundary Conditions for the Unsteady Simulation

For the integrated internal/external thermal flow simulation, pressure far field boundary condition (B.C.) is used for the external field, which includes the flight Mach number, angle of attack and altitude. Pressure inlet B.C. is given at the Piccolo tube holes, where the total pressure and total temperature change with the regulation of the wing anti-icing valve. Symmetrical B.C.'s are applied on the side faces of the external flow field and the sidewalls of the solid skin. Heat transfer is considered for the inner and outer surfaces of the leading edge skin. Other wing surfaces are treated as adiabatic walls.

On the one hand, most of the anti-icing operations are taking place in the second phase climb and initial phase of cruise, and the far field conditions may not vary sharply. On the other hand, the Piccolo tube pressure and temperature will change quickly with the adjustment of the control valves. In the CFD analysis, the Piccolo tube inlet boundary conditions are controlled by using the user-defined functions (UDF). In this approach, the inlet pressure and temperature are described by functions of time written in C⁺⁺ language. In each time step of the flow solution, the B.C. values will be calculated and assigned to the solver automatically.

3.3. Unsteady Simulation with Basic Functions as the Piccolo Tube Inlet Conditions

Most control systems require dynamic input and output variables. In the case of a WAIS, such variables include the pressure and temperature of the piccolo tube, as functions of time. In order to simulate the dynamic functions, one will use the step or exponential

functions for approximation. At the initial step of the unsteady investigation, three such functions are selected to describe the Piccolo tube inlet heat fluxes in a 2D model:

- 1) Single step: $F(X, t) = X_{t=0} + DX, t > 0$
- 2) Exponent law: $F(X, t) = X_{t=0} + DX(1 - \exp(-kt)), k=0.1 \text{ and } 0.5$
- 3) Sin law: $F(X, t) = X_{t=0} + DX \cdot \sin(2\pi kt), k=120$

Where $X=T_0$ and P_0 ; $T_{0 \ t=0} = 453 \text{ K}$, $P_{0 \ t=0} = 90000 \text{ Pa}$; $DT_0 = 5 \text{ K}$, $DP_0 = 2500 \text{ Pa}$ for all the above cases. Meanwhile, the external flow condition is for flight at $M=0.31$, $\alpha=4.5^\circ$ and altitude 6500m.

Fig 4 is a plot of temperature contour of the 2D model at $t=200 \text{ sec}$. In the 2D model, the two staggered rows of small holes on the Piccolo tube are represented with a single slot at zero degree, its width is determined by the sum of the total area of the small holes on the Piccolo tube of one bay. The same assumption is used for the exhaust holes of the bay.

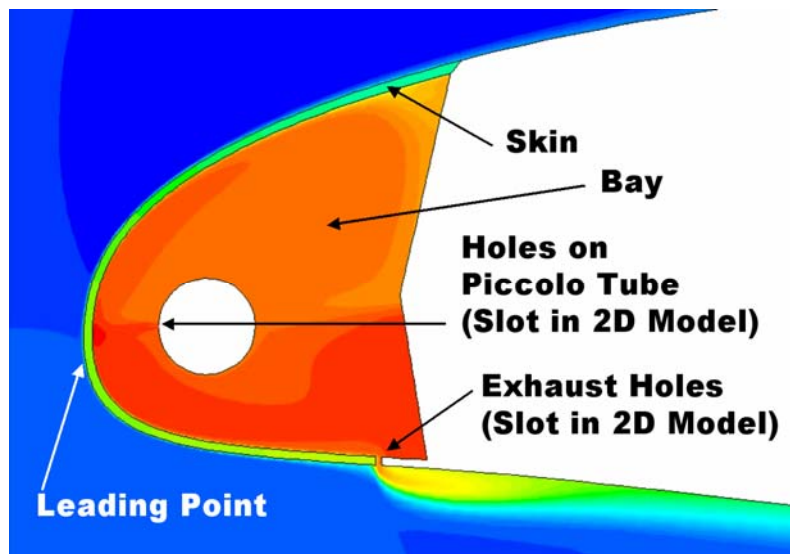


Fig. 4 Temperature contour of the 2D model

This plot shows clearly the hot temperature in the bay, cold external field, skin temperature variation and the merge of the hot exhaust with the external flow.

Fig 5 shows how the temperature of the skin leading point changes with the Piccolo tube inlet conditions for the first two functions.

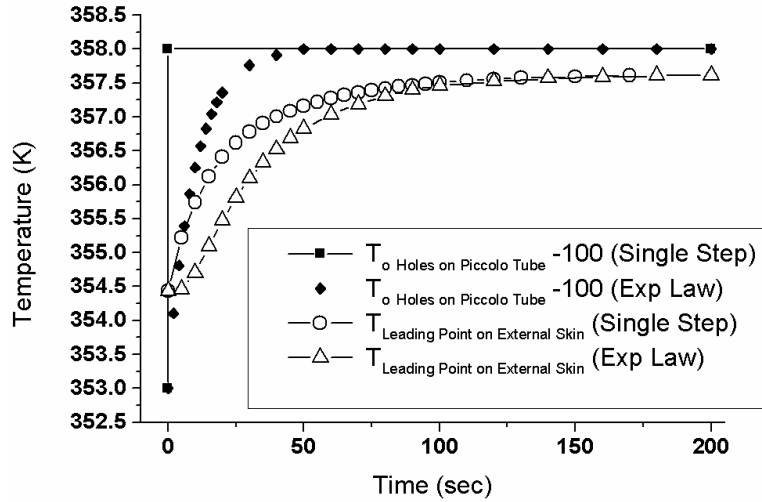


Fig. 5 Skin temperature response to the first two basic functions

Fig. 6 shows the external skin temperature at the leading point varying with the Sin Law in the first 500 seconds.

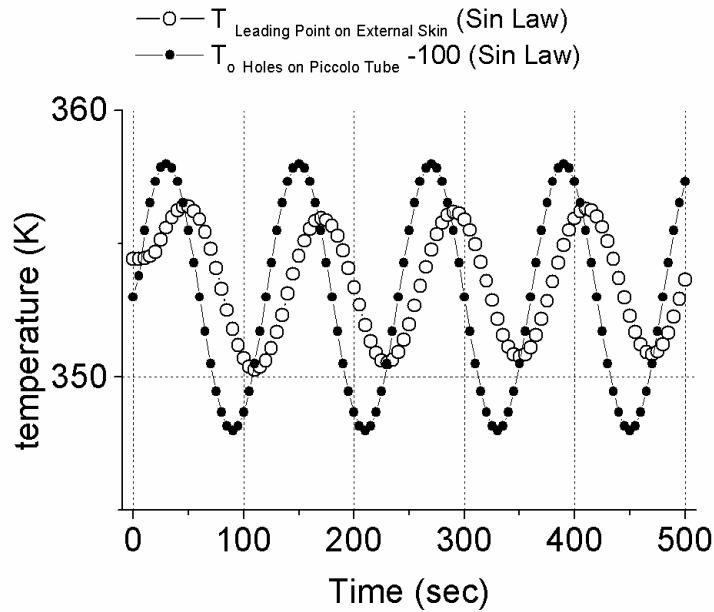


Fig. 6 Response of skin temperature at leading point with Sin Law

Some interesting observations could be collected:

- The temperature histories of the first two functions converge to the same level and at about same time (the curve plotted here for exponent law is $k=0.1$);
- The maximum increase of the skin temperature is about 3 K, lower than the inlet temperature increment of 5 K, indicating the heat loss carried away by the external flows;
- The external skin temperature varies also in Sin law shape in the third case;
- The maximum skin temperature with Sin law is lower than the other two laws as the inlet temperature is changing between +5 and -5 K;
- The maximum and minimum skin temperature with Sin law is increasing slowly as time goes on;
- The maximum (peak) values of the injection speed at the small Piccolo tube holes are about 5 seconds delay than the inlet B.C. values, while the peak skin temperature with Sin law is about 20 seconds delay.

4. Unsteady Thermodynamic Simulation of the WAIS Operation

Based on the above studies of several basic functions, a 3D WAIS thermodynamic CFD model is used to simulate a complete test loop of the anti-icing operation of a BA business jet in dry air flight tests⁹.

In this test segment, the aircraft is in a steady level flight condition. The WAIV opens and regulates the temperature of the heated leading edge in the anti-icing operation for about 350 seconds, and then shuts down. The wing skin would then cool down as the external flow

brings away the remaining heat. Fig 7 shows the measured skin temperature of the process at 83% wing span section. Our task is to simulate this test segment with the CFD model.

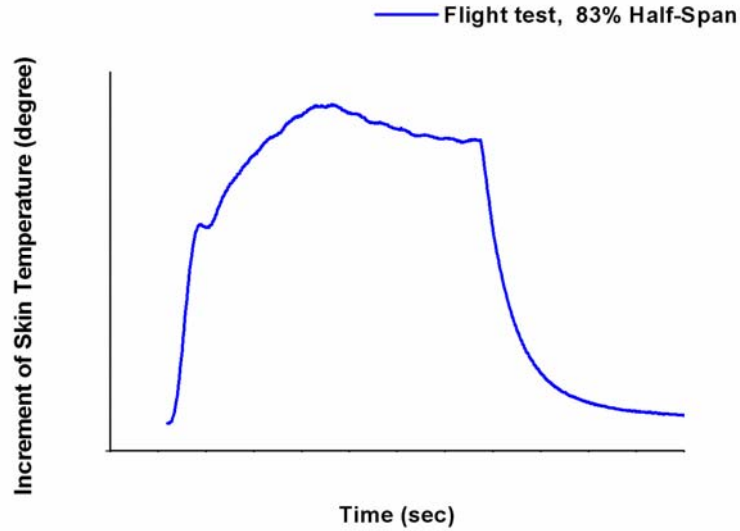


Fig. 7 Measured skin temperatures at leading edge point in anti-icing flight test

4.1. Piccolo Tube Inlet Boundary Conditions for the Simulation

In the flight tests, pressure and temperature are also measured inside the Piccolo tube, as shown in Fig 8 for the pressure at a wing section. These test data are used as the Piccolo tube inlet conditions in the CFD simulation.

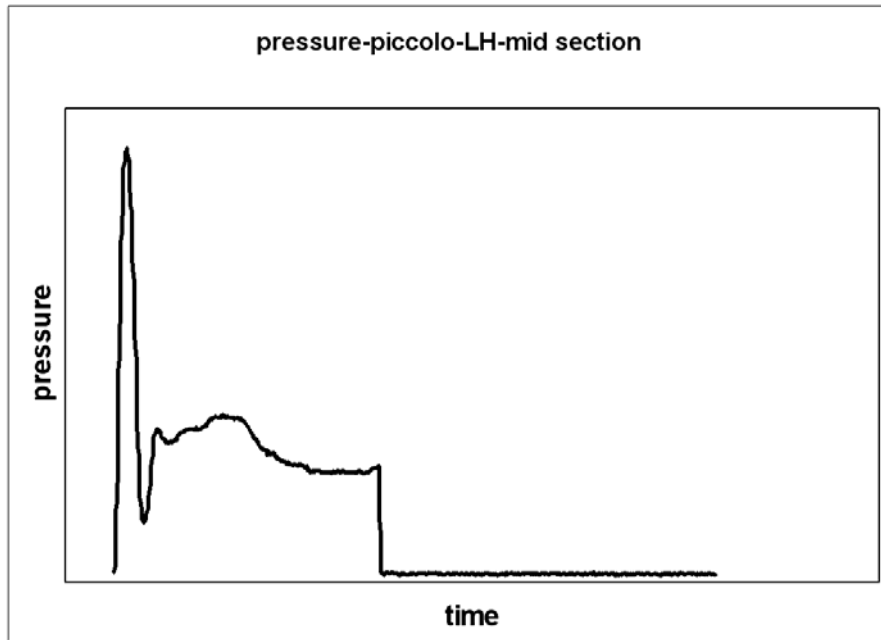


Fig. 8 Measured Piccolo tube pressure in anti-icing flight test

From the plot, it could be seen that there is a sharp pulse in the pressure history when the WAIV just opens, and the pressure also drops sharply when the valve shut down. On the contrary, the temperature changes more smoothly with time. Due to the incontinuity of the curves, the pressure and temperature variations are converted in to four math functions each. The functions to describe the P_0 and T_0 in the Piccolo tube are written as 4 to 6 order polynomials to represent the values for certain time segment. These math functions are written in C++ programs and coupled with the flow solver as user defined functions.

4.2. Numerical Simulation Results

In the simulations, the far field boundary conditions for the external flow are set to be the same as in the flight test. The solver is running in the unsteady implicit segregated

scheme and the Spalart-Allmaras turbulent model is used. Second order upwind schemes are selected. The time step is selected as 0.5 second and there are 50 iterations in each time step.

Fig 9 shows the streamlines of the internal and external flows colored by static temperature. It shows how the hot air impinges the inner skin, flows inside the bay and then merges into the cold external flows through the exhaust holes.

Fig 10 plots the total temperature contours at 10 seconds, where the hot air impingement could be identified very well.

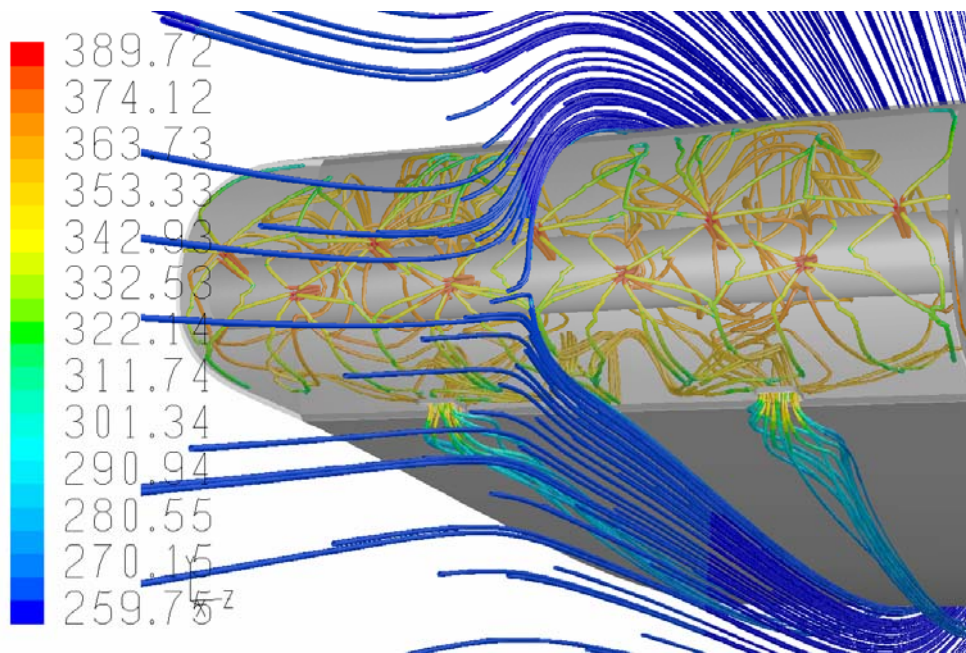


Fig. 9 Streamlines of the CFD simulation colored by temperature (t=36 sec)

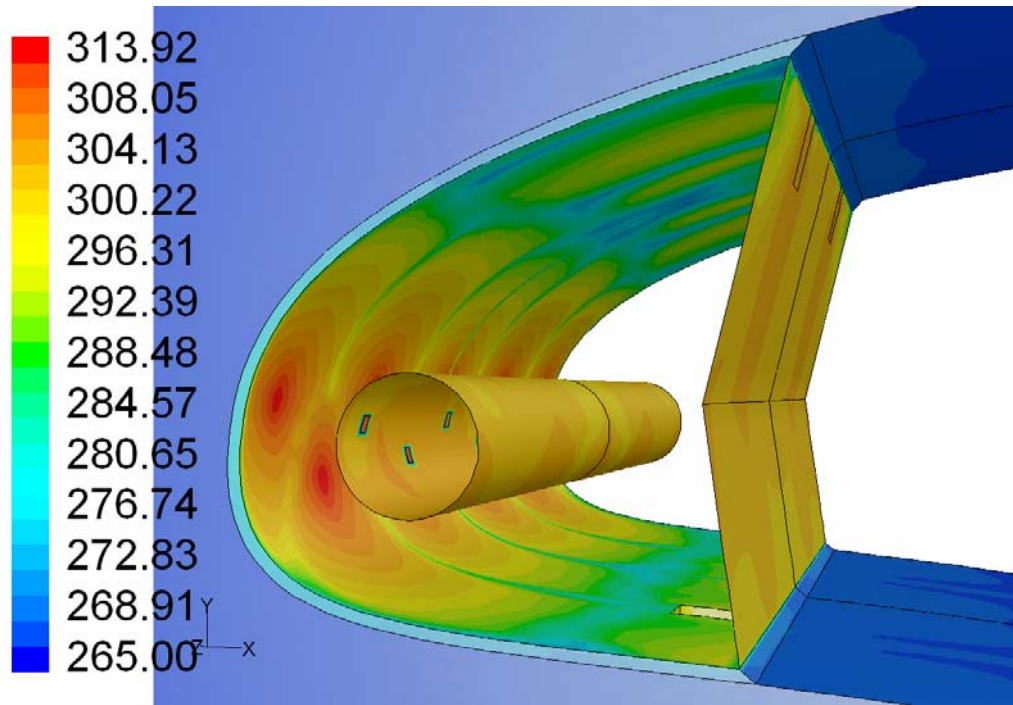
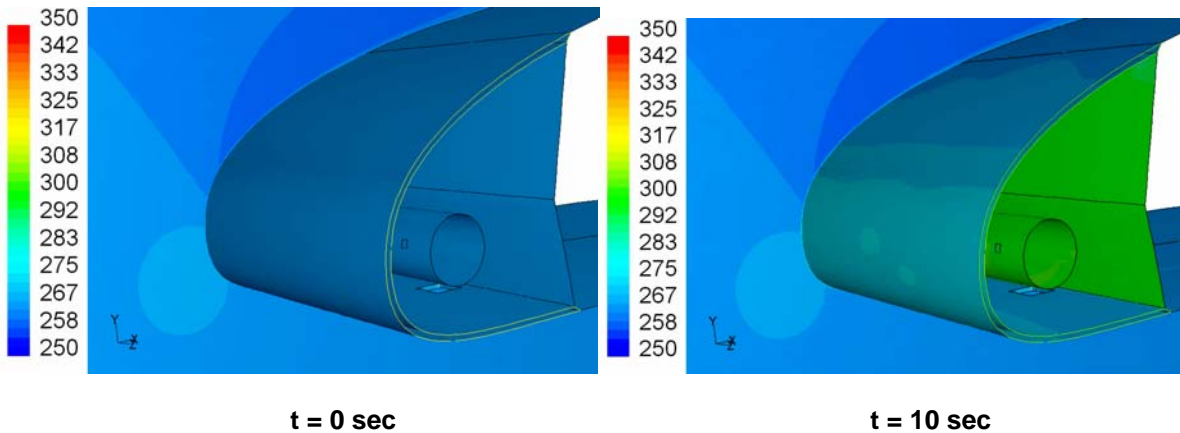


Fig 10 Total temperature contours of the CFD simulation (t=10 sec)

Fig 11 plots the history of the CFD simulated temperature variation at selected time steps through out the test loop. The heating and cold down process could be seen clearly by the color, showing the advantage of the CFD at releasing physical details, which may be expensive to obtain by other measurement techniques.



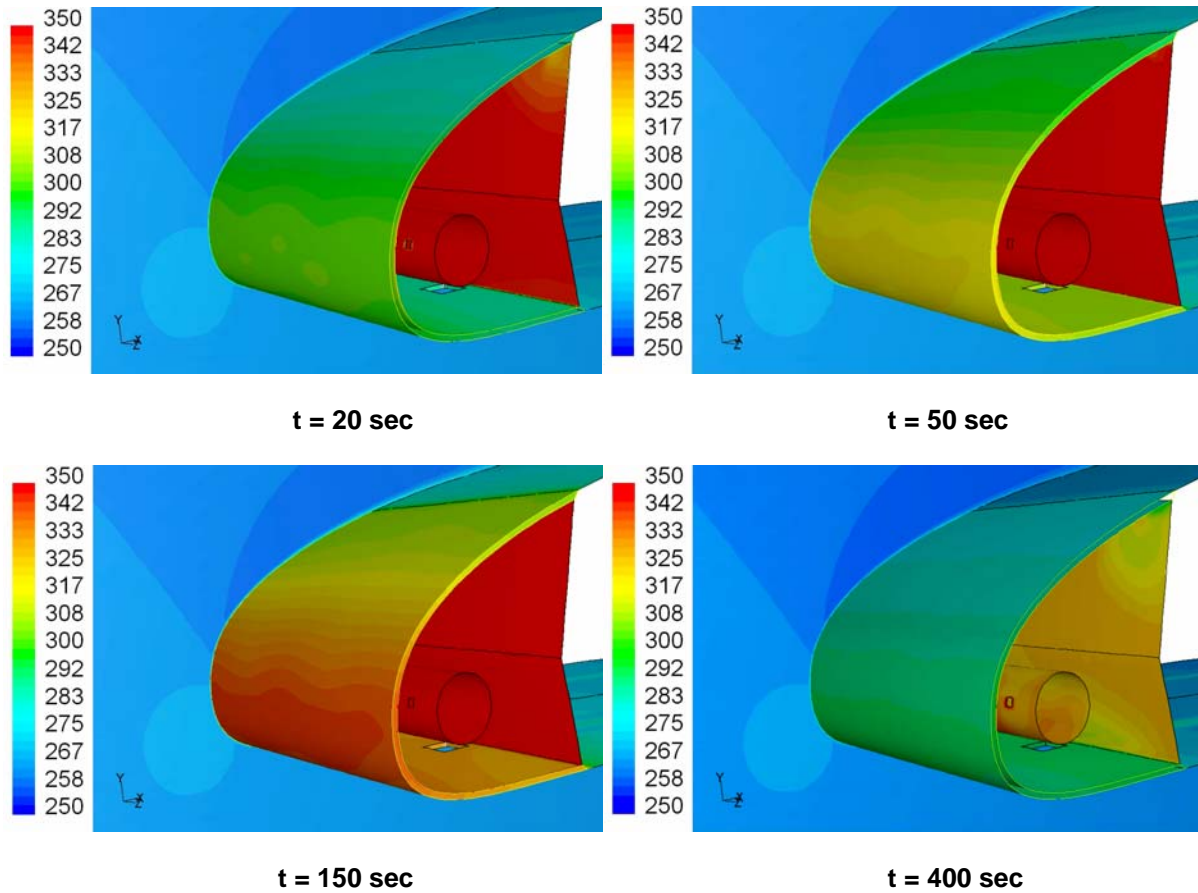


Fig 11 Skin temperature variation history of the CFD simulation (K)

(t=0, 10, 20, 50, 150 and 400 seconds)

4.3 Comparison with Flight Test

Fig 12 compares the 2D and 3D CFD unsteady simulations with flight test. The comparison is for the skin temperature at the leading point of the wing where the sensors are located in the flight test. Flight measured history at two span sections are plotted, even though they are very close to each other.

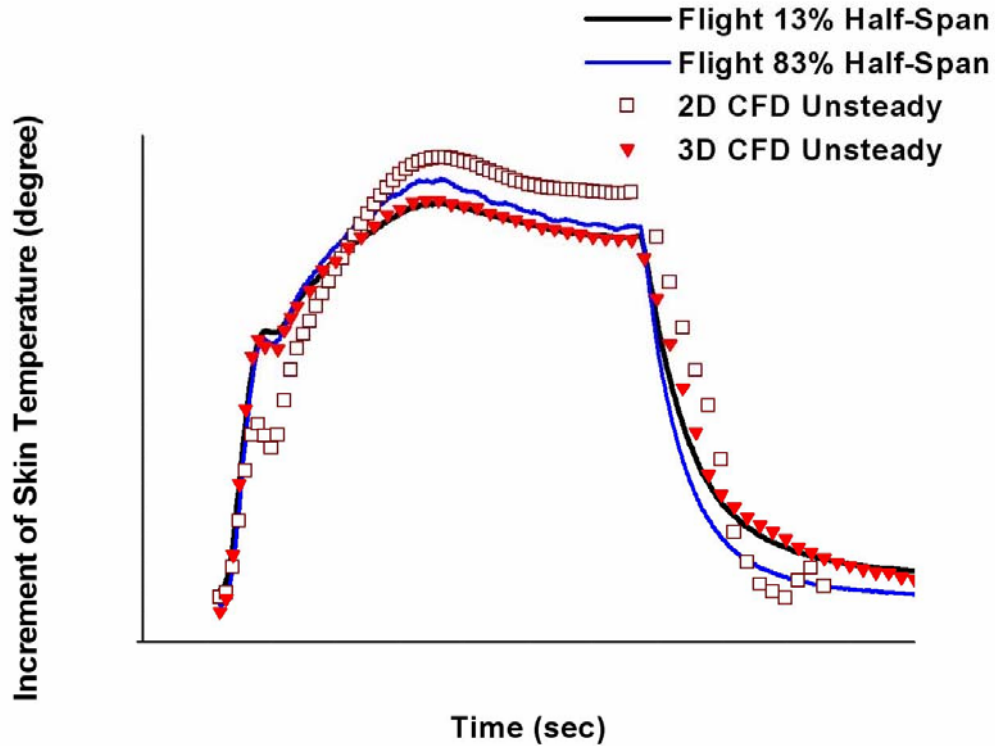


Fig 12 CFD-flight test comparison of skin temperature dynamic variation history

It could be seen that the 3D CFD results have excellent coincidence with the flight test, in the entire time segments from the WAIV opening, regulating and shutting down. The 2D CFD results have under estimation at initial time period and over estimation after the flow is set up. The reason for the under estimation at beginning is because there is only one slot on the Piccolo tube in the 2D model and the leading point is lower than the impingement area of the hot jet; while for the over estimation when the flow is well set up, the flow pattern in the 2D bay section is more stable and there is no cross flow, so the energy is better conserved in the 2D model than in the 3D case. Details of discussion can be found in earlier steady flow simulations ⁶.

5. Conclusions

An aircraft wing anti-icing flight test loop has been represented with a 3D unsteady thermodynamic CFD simulation, based on a Navier-Stokes method, following a 2D unsteady investigation of the same problem.

The heating process is simulated at the beginning of this study by applying different basic functions presenting Piccolo tube heat flux, and the wing skin responses are discussed.

The 3D CFD model involves a complete wing segment with the piccolo type thermal anti-icing bay. In the unsteady integrated internal/external thermal flow simulation with heat conductivity through the solid skin, time dependent boundary condition specifications and proper time steps are investigated. The structured mesh generated increases the unsteady simulations efficiency.

The calculated 3D skin temperature dynamic variation coincides with the flight measurements very well. It indicates the possibility of applying CFD simulation data to the anti-icing system development. It may be used in dynamic model tuning, to complement or even be used in place of the flight test data that are expensive and often not complete enough to serve this purpose. The process of integrating such unsteady CFD simulations into WAIS dynamic model development is currently under investigation.

Acknowledgement

The research work is supported by the Canadian Foundation of Innovation (CFI) and Ontario Innovation Trust (OIT), Ontario Research & Development Challenge Fund (ORDCF) and the Research Grant of the Natural Science and Engineering Council of Canada (NSERC). The CFI/OIT funds are partially supported by the generous endowments of the Bombardier Foundation. The authors would like to express their appreciation to Bombardier Aerospace for providing access to some flight test data. The authors would also like to thank Dr. Ahmed Hassan, the Associate Editor, and the anonymous reviewers for their constructive comments to the original manuscript.

References

1. Bourgault, Y., Boutanios, Z. and Habashi, W.G., “Three-dimensional Eulerian Approach to Droplet Impingement Simulation Using FENSAP-ICE, Part1: Model, Algorithm, and Validation”, *Journal of Aircraft*, Vol. 37, No. 1, pp 95-103, 2000.
2. Beaugendre, H., Morency, F. and Habashi, W.G., “FENSAP-ICE’s Three-Dimensional In-Flight Ice Accretion Module: ICE3D”, *Journal of Aircraft*, Vol.40, No.2, pp 239-247, 2003.
3. Bidwell, C.S., Pinella, D. and Garrison, P., “Ice Accretion Calculations for a Commercial Transport Using the LEWICE3D, ICEGRID3D and CMARC Programs”, NASA/TM-1999-208895, 1999.
4. Morency, F., Tezok, F. and Paraschivoiu, I., “Heat and Mass Transfer in the Case of Anti-Icing System Simulation”, *Journal of Aircraft*, Vol. 37, No.2, pp245-252, 2000.

5. de Mattos, B.S. and Oliveira, G.L., “Three-dimensional Thermal Coupled Analysis of a Wing Slice Slat with a Piccolo Tube”, AIAA-2000-3921, 2000.
6. Liu, H.H.T. and Hua, J., “Three-Dimensional Integrated Thermodynamic Simulation for Wing Anti-Icing System”, Journal of Aircraft, Vol. 41, No. 6, pp 1291-1297, 2004.
7. Hua, J. and Liu, H.H.T., “Fluid Flow and Thermodynamic Analysis of a Wing Anti-Icing System”, Canadian Aeronautics and Space Journal, Vol. 51, No. 1, pp 35-40, 2005.
8. Fluent V6 User Guide, 2003.
9. Bombardier Aerospace, “Flight Test Data of Wing Anti-Icing System”, Internal Communication, 2003.